

# Fundamental difference in the electronic reconstruction of infinite-layer vs. perovskite neodymium nickelate films on SrTiO<sub>3</sub>(001)

Benjamin Geisler\* and Rossitza Pentcheva†

Department of Physics and Center for Nanointegration (CENIDE),  
Universität Duisburg-Essen, Lotharstr. 1, 47057 Duisburg, Germany

(Dated: September 2, 2022)

Motivated by the recent reports of superconductivity in Sr-doped NdNiO<sub>2</sub> films on SrTiO<sub>3</sub>(001) [Li *et al.*, Nature (London) 572, 624 (2019)], we explore the role of the polar interface on the structural and electronic properties of NdNiO<sub>n</sub>/SrTiO<sub>3</sub>(001) ( $n = 2, 3$ ) by performing first-principles calculations including a Coulomb repulsion term. For infinite-layer nickelate films ( $n = 2$ ), electronic reconstruction drives the emergence of a two-dimensional electron gas (2DEG) at the interface involving a strong occupation of the Ti 3d states. This effect is more pronounced than in the paradigmatic LaAlO<sub>3</sub>/SrTiO<sub>3</sub>(001) system and accompanied by a substantial reconstruction of the Fermi surface as well as strong ionic relaxations and Ni valence modulations. The Ni  $e_g$  orbital polarization increases throughout the film and exceeds 35% at the surface. In contrast, no 2DEG forms for films in the perovskite structure ( $n = 3$ ) or if a single perovskite layer persists at the interface, and the polarity mismatch is exclusively accommodated by electrostatic doping of the nickelate, accompanied by ionic relaxations. We analyze the topotactic reaction from the perovskite to the infinite-layer phase and show why the reduction is confined to the nickelate film, whereas the SrTiO<sub>3</sub> substrate remains intact.

Interface polarity plays a key role in transition metal oxide heterostructures, since it can drive the emergence of physical properties that are absent in the respective bulk compounds [1–3]. A prominent example is the LaAlO<sub>3</sub>/SrTiO<sub>3</sub>(001) system (LAO/STO [4, 5]), in which a correlated two-dimensional electron gas (2DEG) is formed at the interface by occupation of Ti 3d conduction band states beyond 4 unit cells of LAO [6, 7] that shows intriguing physics, for instance, superconductivity [8]. Electronic reconstructions such as this can accommodate the polarity mismatch and thereby circumvent the polar catastrophe, i.e., the infinite build-up of electrostatic potential [5, 9].

The very recent observation of superconductivity in Sr-doped NdNiO<sub>2</sub> films grown on STO(001) by Li *et al.* [10] has sparked considerable interest in infinite-layer nickelates, since their formal Ni<sup>1+</sup> (3d<sup>9</sup>) valence state renders them close to cuprates. Most of the theoretical efforts to explain the phenomenon so far have concentrated on the electronic properties of bulk compounds [11–15]. However, superconductivity could not be confirmed experimentally in Sr-doped bulk NdNiO<sub>2</sub> [16]. This raises a question about the role of the interface to the substrate that has hardly been addressed so far.

Here we explore the impact of the polar interface on the structural and electronic properties of NdNiO<sub>n</sub>/STO(001) ( $n = 2, 3$ ) by performing first-principles calculations including a Coulomb repulsion term and find it to play a decisive role. While polar discontinuities exist at interface and surface in both the infinite-layer ( $n = 2$ ) and the perovskite ( $n = 3$ ) films, we find the accommodation mechanism to be highly different. The simulations unravel a clear 2DEG formation for  $n = 2$  due to a strong occupation of interfacial Ti, predominantly 3d<sub>xy</sub> states, and more pronounced than in LAO/STO(001). The 2DEG forms already for a single unit cell of infinite-layer nickelate on STO(001). At the interface, the missing apical oxygen modifies the crystal field splitting, which leads to a partial occupation of Ti  $d_{z^2}$  states and thus to

a finite Ti  $e_g$  orbital polarization of  $\sim 12\%$ . Moreover, we observe a modulation of the Ni  $e_g$  orbital polarization throughout the nickelate film that increases from  $\sim 12\%$  at the interface to large values  $> 35\%$  at the surface. The electronic reconstruction is accompanied by a substantial reconstruction of the Fermi surface as well as strong ionic relaxations and Ni valence modulations. In sharp contrast, for  $n = 3$  the Ti 3d states remain empty, and the polarity mismatch is exclusively accommodated by electrostatic doping of the nickelate, accompanied by ionic relaxations. Interestingly, the formation of a 2DEG is inhibited even if a single perovskite layer persists at the interface. In that case, strong octahedral rotations are induced at the interface that are driven out in ideal infinite-layer nickelate films. Finally, we analyze the oxygen deintercalation reaction and show why the reduction is confined to the nickelate film. These insights may be of key importance for a fundamental understanding of superconductivity in infinite-layer nickelates.

**Methodology.** — We performed first-principles calculations in the framework of density functional theory [17] (DFT) as implemented in the Quantum ESPRESSO code [18]. The generalized gradient approximation was used for the exchange-correlation functional as parametrized by Perdew, Burke, and Ernzerhof [19]. Static correlation effects were considered within the DFT+ $U$  formalism [20] employing  $U = 4$  eV on Ni and Ti sites, in line with previous work [15, 21–25]. We model (NdNiO<sub>n</sub>)<sub>m</sub>/STO(001) ( $n = 2, 3$ ) by using  $\sqrt{2}a \times \sqrt{2}a$  supercells with two transition metal sites per layer to account for octahedral rotations, strained to the STO substrate lattice parameter 3.905 Å. The supercells contain 5 layers of STO substrate and  $m = 1$ -6 layers of nickelate film, subsequently doubled to obtain symmetric slabs (the figures only show half of the supercell). The vacuum region spans 20 Å. We focus here on structural and electrostatic effects and therefore discuss nonmagnetic results in the following [10, 26], noting that spin-polarized calculations with ferromagnetic or A-

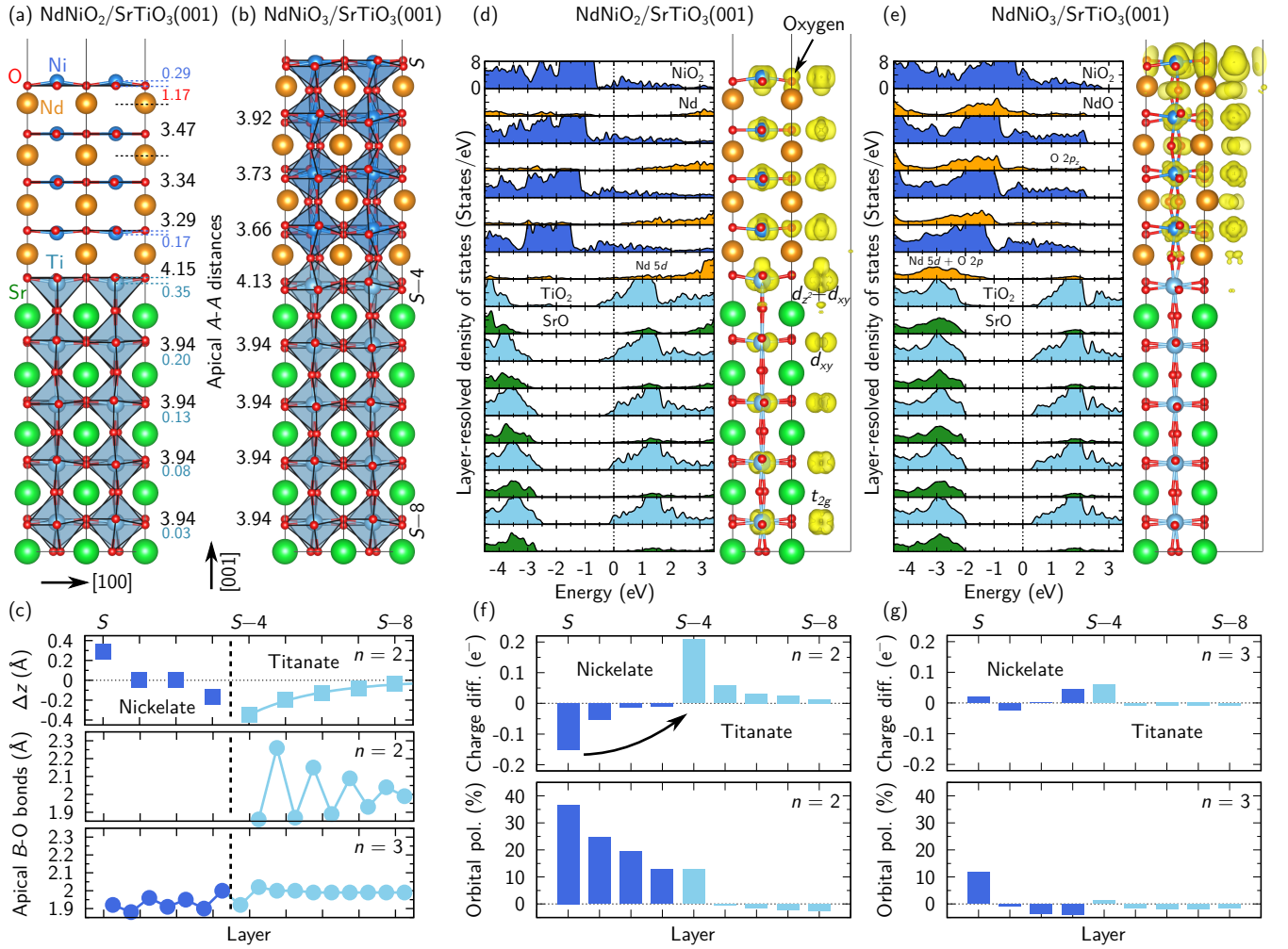


Figure 1. (a, b) Optimized geometry of  $(\text{NdNiO}_n)_4/\text{STO}(001)$  ( $n = 2$ : infinite-layer;  $n = 3$ : perovskite). (c) The vertical displacements  $\Delta z$  of the B site ions from their respective oxygen layers are substantial for  $n = 2$ ; for  $n = 3$ , they are negligible (not shown). The apical B-O bond lengths reflect the highly distinct ionic relaxation in the two systems. (d, e) Corresponding layer-resolved density of states and distribution of electron density (integrated between  $-0.7$  eV and  $E_F$ ), visualizing the fundamental differences in electronic reconstruction. The strong oxygen contributions to the electron density in the nickelate region (absent in STO) highlight its covalent nature. (f, g) Layer-resolved charge difference at Ni and Ti sites relative to the respective bulk compounds and Ni and Ti  $e_g$  orbital polarization of  $(\text{NdNiO}_n)_4/\text{STO}(001)$ . The former show the valence modulations arising particularly for  $n = 2$ . A positive orbital polarization indicates a preferential  $3d_{z^2}$  occupation.

and G-type antiferromagnetic order in the nickelate films resulted in qualitatively identical results with respect to 2DEG formation for both  $n = 2$  and  $n = 3$ . Wave functions and density were expanded into plane waves up to cutoff energies of 45 and 350 Ry, respectively. Ultrasoft pseudopotentials [27] as successfully employed in previous work [22–25, 28–30], were used in conjunction with projector augmented wave datasets [31]. The Nd 4f electrons are frozen in the core [11, 21]. We used a  $12 \times 12 \times 1$  Monkhorst-Pack  $\vec{k}$ -point grid [32] and 5 mRy Methfessel-Paxton smearing [33] to sample the Brillouin zone. The ionic positions were accurately optimized, reducing ionic forces below 1 mRy/a.u.

**Ionic relaxation.** — We focus our discussion on  $(\text{NdNiO}_n)_4/\text{STO}(001)$  heterostructures with a representative film thickness of 4 unit cells. The lattice parameters of bulk

$\text{NdNiO}_2$  ( $a = 3.92$ ,  $c = 3.28$  Å [11, 34]) imply that the film is subject to compressive strain if grown epitaxially on  $\text{STO}(001)$  [ $a = 3.905$  Å, Fig. 1(a)]. Consequently, the infinite-layer film expands vertically ( $\sim 2.6\%$ ). Interestingly, we find that this expansion is not homogeneous; instead, the distances between the distinct Nd layers increase continuously from the interface (3.29 Å) to the surface (3.47 Å). An analogous trend is observed for the perovskite film [ $n = 3$ , tensile strain, Fig. 1(b)] with even larger distances. The Nd-Sr distance at the interface is particularly enhanced for the infinite-layer film (4.15 Å), slightly more pronounced than for the perovskite film (4.13 Å). A similar expansion at the interface (4.06 Å) has been observed in  $n$ -type  $(\text{LaNiO}_{3.5}/\text{STO})_{2.5}(001)$  superlattices on  $\text{STO}(001)$  [22].

The perovskite film exhibits considerable octahedral rota-

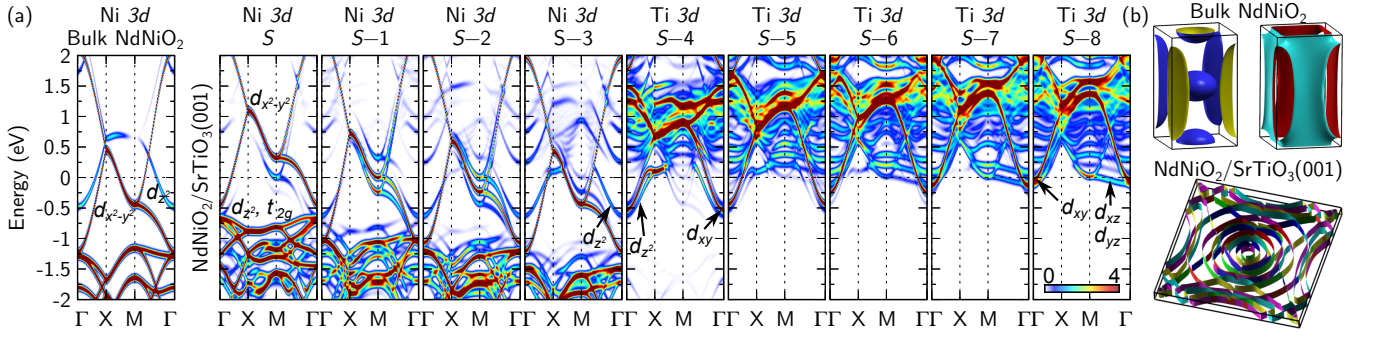


Figure 2. (a) Band structures (i.e.,  $\vec{k}$ -resolved densities of states, projected on Ni 3d and Ti 3d orbitals in different layers) of (NdNiO<sub>2</sub>)<sub>4</sub>/STO(001). For reference, a panel for bulk NdNiO<sub>2</sub> is provided. The orbital characters are denoted. (b) The film Fermi surface is considerably reconstructed with respect to the bulk Fermi surface, which consists of two sheets and is calculated here by using a comparable  $\sqrt{2} \times \sqrt{2}$  cell. The Fermi surface of bulk NdNiO<sub>2</sub> closely resembles that of LaNiO<sub>2</sub> [15, 35].

tions [Fig. 1(b)], particularly at the interface with an apical Ni-O-Ti bond angle of  $155^\circ$  and basal Ni-O-Ni and Ti-O-Ti bond angles of  $155.5^\circ$  and  $157.7^\circ$ , respectively. We find the rotational pattern of bulk NdNiO<sub>3</sub> ( $a^- a^- c^+$ ) to be reflected in the film geometry. Owing to the octahedral connectivity, the rotations in the film extend into the STO substrate. In contrast, in the infinite-layer heterostructure, the small intrinsic octahedral rotations of STO are removed near the interface, and the NiO<sub>4</sub> squares show no rotations around the  $c$  axis [Fig. 1(a)].

For  $n = 2$ , the central NiO<sub>2</sub> layers are coplanar, whereas the surface (interface) layer is buckled, the Ni ion being vertically displaced outwards (inwards) from the respective oxygen layer by  $\Delta z = 0.29 \text{ \AA}$  ( $-0.17 \text{ \AA}$ ), a response to the internal electric field build-up in the polar films [Fig. 1(a,c)]. The distance between the surface NiO<sub>2</sub> layer and the subsurface Nd layer is considerably contracted and amounts to only  $1.17 \text{ \AA}$ . The Ti ions in the STO substrate show a sizeable inwards vertical displacement (away from the interface), particularly at the interface ( $\Delta z \sim -0.35 \text{ \AA}$ ), that decays exponentially as  $\Delta z \approx -0.35 \text{ \AA} \cdot \exp(-d/7.42 \text{ \AA})$  with the distance  $d$  to the interfacial TiO<sub>2</sub> layer [ $S-4$ ; Fig. 1(c)]. This trend is also expressed in strong oscillations of the apical Ti-O bond lengths around the bulk value [ $1.96 \text{ \AA}$ ; Fig. 1(c)]. Our observations for  $n = 3$  are in sharp contrast: In the nickelate, the Ni displacements are smaller than  $0.05 \text{ \AA}$ ; in the STO substrate, the Ti displacements almost vanish. This qualitatively different structural response to the polar discontinuities in infinite-layer vs. perovskite nickelate films points at fundamentally distinct accommodation mechanisms, which we unravel in the following.

**Electronic reconstruction.** — For infinite-layer nickelate films ( $n = 2$ ), we observe a considerable electronic reconstruction. The polar discontinuities at the interface and the surface induce a substantial charge transfer, expressed in a depletion (relative to bulk) at the Ni sites (i.e., of the delocalized NiO<sub>2</sub> bands), in particular at the surface, whereas the Ti ions gain charge in the localized 3d states, particularly at the interface, with rapid decay into the substrate [Fig. 1(d,f)]. A 2DEG emerges at the interface with considerable band bending in the

nickelate film and the STO substrate, as can be seen from the layer-resolved density of states [Fig. 1(d)] and the band structure [Fig. 2(a)]. The strong Ti 3d occupation at the interface is in stark contrast with (LaO)<sub>4</sub>/STO(001), which is just at the verge of a metal-insulator transition [7]. Already for ultra-thin (NdNiO<sub>2</sub>)<sub>1</sub>/STO(001) films, we observe a 2DEG, albeit with reduced Ti 3d occupation ( $-0.076 e^-$  at the interface). In contrast, increasing the film thickness from 4 to 6 layers induces only negligible changes in the surface and interface electronic structure. Since the apical Ti-O bond length at the interface is contracted [ $1.86 \text{ \AA}$ , Fig. 1(c)] relative to STO bulk ( $1.96 \text{ \AA}$ ), predominantly the  $3d_{xy}$  orbital gets occupied due to its lowered energy. This can clearly be seen in the distribution of electron density [Fig. 1(d)] and resembles the situation in LAO/STO(001) [36, 37]. This orbital order persists for three layers and then develops into a uniform occupation of the  $t_{2g}$  manifold.

In contrast, we find no tendency towards 2DEG formation in the perovskite ( $n = 3$ ) heterostructures and only negligible charge redistribution, as shown for the representative (NdNiO<sub>3</sub>)<sub>4</sub>/STO(001) system in Fig. 1(e,g), despite a clearly visible electric field in the layer-resolved density of states of the film.

In addition to the charge transfer, we observe a strong modulation of the Ni  $e_g$  orbital polarization throughout the infinite-layer nickelate films [Fig. 1(f)] defined from the orbital occupations  $n$  by  $P = (n_{3d_{z^2}} - n_{3d_{x^2-y^2}})/(n_{3d_{z^2}} + n_{3d_{x^2-y^2}})$  and increasing from the interface ( $P \sim 12\%$ ) to the surface ( $P > 35\%$ ), indicating a preferential occupation of the  $3d_{z^2}$  orbitals. These values exceed attainable values in nickelate/aluminate SLs on a variety of different substrates [25, 38–40]; the incomplete orbital polarization has been discussed as a major hindrance for superconductivity [10]. For reference, in bulk NdNiO<sub>2</sub> we find a Ni  $e_g$  orbital polarization of 17%. Interestingly, even the interfacial Ti ions exhibit a finite orbital polarization ( $P \sim 12\%$ ) due to a partial occupation of the  $3d_{z^2}$  orbital. Again, the behavior of perovskite films is distinct, with only moderate orbital polarization ( $P \sim 11\%$ ) exclusively at the surface [Fig. 1(g)].



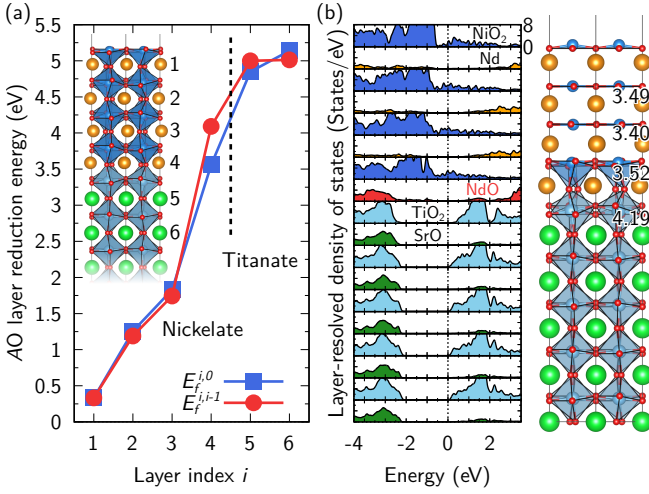


Figure 3. (a) Energies  $E_f^{i,0}$  and  $E_f^{i,i-1}$  (per formula unit; see text) required to reduce different AO layers in  $(\text{NdNiO}_3)_4/\text{STO}(001)$  heterostructures ( $A = \text{Nd, Sr}$ ). (b) Electronic structure and optimized geometry of  $(\text{NdNiO}_2)_3/(\text{NdNiO}_3)_1/\text{STO}(001)$ . The oxidized layer at the interface (marked in red) inhibits the formation of a 2DEG.

The layer-resolved band structures in Fig. 2(a) show that at the interface, the Ti  $3d_{xy}$  band is bent down to  $\sim -0.55$  eV at the  $\Gamma$  point. Moreover, we observe a hybridized Ni  $3d_{z^2}$ –Ti  $3d_{z^2}$  state at the interface, visible for instance at  $\sim -0.65$  eV at the  $\Gamma$  point, that extends into the nickelate. In the surface layer, the Ni  $3d$  bands are only occupied around the  $\Gamma$  point; from the subsurface layer on, also an electron pocket around the  $M$  point emerges. In the STO region, only an electron pocket around the  $\Gamma$  point is occupied, having  $3d_{xy} + 3d_{z^2}$  character at the interface and  $3d_{xy} + 3d_{xz} + 3d_{yz}$  character deeper in the substrate. Therefore, the Fermi surfaces of infinite-layer heterostructures experience considerable reconstructions with respect to bulk [Fig. 2(b)].

Interestingly, the Nd  $5d$  states, which might be relevant for the superconductivity mechanism [26], are strongly affected by the band bending. The layer-resolved density of states for  $n = 2$  shows that the Nd  $5d$  states are generally empty and  $\sim 2$  eV above  $E_F$  near the surface [Fig. 1(d)]. Only at the interface, they are bent down to  $\sim -0.6$  eV, leading to a small but finite occupation as reported for bulk  $\text{NdNiO}_2$  [11]. Therefore, their contribution to the conductivity of a real heterostructure is much smaller than expected from bulk. For  $n = 3$ , occupied Nd  $5d$ –O  $2p_{x,y}$  hybrid states form  $\sim 1$  eV below the Fermi energy at the interface that reach up to the Fermi energy near the surface [Fig. 1(e)].

**Oxygen deintercalation.** — We now address the topotactic oxygen deintercalation reaction from the perovskite to the infinite-layer phase. As a first approach, Fig. 3(a) displays single-layer reduction energies (i.e., apical oxygen vacancy layer formation energies), defined from DFT total energies as  $E_f^{i,0} = E_{\text{single layer } i \text{ reduced}} - E_{\text{ideal perovskite film}} + \mu_O$  with  $\mu_O = \frac{1}{2}E_{\text{O}_2}$ , i.e., in the oxygen-rich limit. The formation energies are lowest at the surface ( $\sim 0.5$  eV) and increase to  $\sim$

1.8 eV in the third layer. At the interface, the oxygen ions are moderately bound ( $\sim 3.5$  eV), and very strongly in the STO substrate ( $> 4.8$  eV). This is in line with an oxygen vacancy formation energy of  $\sim 5.5$  eV in bulk STO [41] and comparable to values near the LAO/STO(001) interface [42]. The values in nickelates are generally lower (e.g., bulk  $\text{LaNiO}_3$ :  $2.8 \pm 0.2$  eV [43],  $(\text{LaNiO}_3)_3/(\text{LAO})_1(001)$  superlattices on STO(001): 2.3 eV [25]). The nickelate layers are therefore easily reduced, whereas oxygen deintercalation in the STO substrate is inhibited by the high formation energies.

In a second and more realistic approach, we model successive layer-by-layer reduction,  $E_f^{i,i-1} = E_{\text{topmost } i \text{ layers reduced}} - E_{\text{topmost } i-1 \text{ layers reduced}} + \mu_O$ , which largely concurs with the results of the first approach. Peculiarly, we find that the oxygen binding is enhanced at the interface if the above nickelate layers are already reduced. This leads to the surprising situation that the interfacial Nd layer may retain its oxygen under appropriately chosen experimental conditions. Figure 3(b) shows the corresponding electronic structure and optimized geometry. The single non-reduced (i.e., perovskite) layer at the interface inhibits the formation of a 2DEG. Instead, the STO conduction band aligns with the Fermi energy, and only little band bending can be observed directly at the interface. No layer exhibits Nd  $5d$  states near the Fermi energy. While for ideal infinite-layer films the octahedral rotations are removed at the interface [Fig. 1(a)], here they are enhanced even beyond values of perovskite films. The Nd layer distances show ionic relaxations of comparable magnitude to the ideal infinite-layer case. The NdO–Nd layer distance at the interface (3.52 Å) is considerably larger (smaller) than for ideal infinite-layer (perovskite) films and thus may act as a fingerprint in transmission electron microscopy to detect the interface layer stacking even if oxygen sites are difficult to resolve.

**Summary.** — We investigated the electronic reconstructions in  $\text{NdNiO}_n/\text{SrTiO}_3(001)$  ( $n = 2, 3$ ) driven by interface polarity from first-principles. The results show that the polar discontinuities at the interface and the surface considerably affect the electronic structure throughout infinite-layer nickelate films and several layers (at least 5 unit cells) into the STO substrate. Moreover, the accommodation mechanism is fundamentally different for infinite-layer and perovskite nickelates. The substantial modulations of the Ni and Ti valence and orbital polarization observed for the infinite-layer films on  $\text{SrTiO}_3(001)$  are likely to impact superconductivity considerably, which implies that modeling the epitaxial films simply as strained bulk is only of limited relevance. Hence, interface polarity emerges as a key aspect in understanding superconductivity in infinite-layer nickelates and requires further consideration in future studies. Parallels to other superconducting systems such as LAO/STO(001) [8] and FeSe/STO(001) [44] may point to a more general phenomenon.

## ACKNOWLEDGMENTS

This work was supported by the German Research Foundation (Deutsche Forschungsgemeinschaft, DFG) within the SFB/TRR 80 (Projektnummer 107745057), Project No. G3. Computing time was granted by the Center for Computational Sciences and Simulation of the University of Duisburg-Essen (DFG Grants No. INST 20876/209-1 FUGG and No. INST 20876/243-1 FUGG).

\* [benjamin.geisler@uni-due.de](mailto:benjamin.geisler@uni-due.de)

† [rossitza.pentcheva@uni-due.de](mailto:rossitza.pentcheva@uni-due.de)

- [1] J. Mannhart and D. G. Schlom, *Science* **327**, 1607 (2010).
- [2] H. Y. Hwang, Y. Iwasa, M. Kawasaki, B. Keimer, N. Nagaosa, and Y. Tokura, *Nat. Mater.* **11**, 103 (2012).
- [3] A. Ohtomo, D. A. Muller, J. L. Grazul, and H. Y. Hwang, *Nature* **419**, 378 (2002).
- [4] A. Ohtomo and H. Y. Hwang, *Nature* **427**, 423 (2004).
- [5] N. Nakagawa, H. Y. Hwang, and D. A. Muller, *Nat. Mater.* **5**, 204 (2006).
- [6] S. Thiel, G. Hammerl, A. Schmehl, C. W. Schneider, and J. Mannhart, *Science* **313**, 1942 (2006).
- [7] R. Pentcheva and W. E. Pickett, *Phys. Rev. Lett.* **102**, 107602 (2009).
- [8] N. Reyren, S. Thiel, A. D. Caviglia, L. F. Kourkoutis, G. Hammerl, C. Richter, C. W. Schneider, T. Kopp, A.-S. Rüetschi, D. Jaccard, M. Gabay, D. A. Muller, J.-M. Triscone, and J. Mannhart, *Science* **317**, 1196 (2007).
- [9] C. Noguera, *J. Phys.: Condens. Matter* **12**, R367 (2000).
- [10] D. Li, K. Lee, B. Y. Wang, M. Osada, S. Crossley, H. R. Lee, Y. Cui, Y. Hikita, and H. Y. Hwang, *Nature* **572**, 624 (2019).
- [11] Y. Nomura, M. Hirayama, T. Tadano, Y. Yoshimoto, K. Nakamura, and R. Arita, *Phys. Rev. B* **100**, 205138 (2019).
- [12] P. Jiang, L. Si, Z. Liao, and Z. Zhong, *Phys. Rev. B* **100**, 201106 (2019).
- [13] H. Sakakibara, H. Usui, K. Suzuki, T. Kotani, H. Aoki, and K. Kuroki, (2019), [arXiv:1909.00060 \[cond-mat.supr-con\]](https://arxiv.org/abs/1909.00060).
- [14] M. Jiang, M. Berciu, and G. A. Sawatzky, (2019), [arXiv:1909.02557 \[cond-mat.supr-con\]](https://arxiv.org/abs/1909.02557).
- [15] A. S. Botana and M. R. Norman, (2019), [arXiv:1908.10946 \[cond-mat.supr-con\]](https://arxiv.org/abs/1908.10946).
- [16] Q. Li, C. He, J. Si, X. Zhu, Y. Zhang, and H.-H. Wen, (2019), [arXiv:1911.02420 \[cond-mat.supr-con\]](https://arxiv.org/abs/1911.02420).
- [17] W. Kohn and L. J. Sham, *Phys. Rev.* **140**, A1133 (1965).
- [18] P. Giannozzi, S. Baroni, N. Bonini, M. Calandra, R. Car, C. Cavazzoni, D. Ceresoli, G. L. Chiarotti, M. Cococcioni, I. Dabo, A. Dal Corso, S. de Gironcoli, S. Fabris, G. Fratesi, R. Gebauer, U. Gerstmann, C. Gougoussis, A. Kokalj, M. Lazzeri, L. Martin-Samos, N. Marzari, F. Mauri, R. Mazzarello, S. Paolini, A. Pasquarello, L. Paulatto, C. Sbraccia, S. Scandolo, G. Sclauzero, A. P. Seitsonen, A. Smogunov, P. Umari, and R. M. Wentzcovitch, *J. Phys.: Condens. Matter* **21**, 395502 (2009).
- [19] J. P. Perdew, K. Burke, and M. Ernzerhof, *Phys. Rev. Lett.* **77**, 3865 (1996).
- [20] M. Cococcioni and S. de Gironcoli, *Phys. Rev. B* **71**, 035105 (2005).
- [21] J. Liu, M. Kargarian, M. Kareev, B. Gray, P. J. Ryan, A. Cruz, N. Tahir, Y.-D. Chuang, J. Guo, J. M. Rondinelli, J. W. Freeland, G. A. Fiete, and J. Chakhalian, *Nature Communications* **4**, 2714 (2013).
- [22] B. Geisler, A. Blanca-Romero, and R. Pentcheva, *Phys. Rev. B* **95**, 125301 (2017).
- [23] F. Wrobel, B. Geisler, Y. Wang, G. Christiani, G. Logvenov, M. Bluschke, E. Schierle, P. A. van Aken, B. Keimer, R. Pentcheva, and E. Benckiser, *Phys. Rev. Materials* **2**, 035001 (2018).
- [24] B. Geisler and R. Pentcheva, *Phys. Rev. Materials* **2**, 055403 (2018).
- [25] B. Geisler and R. Pentcheva, *Phys. Rev. Applied* **11**, 044047 (2019).
- [26] G. A. Sawatzky, *Nature* **572**, 592 (2019).
- [27] D. Vanderbilt, *Phys. Rev. B* **41**, 7892 (1990).
- [28] B. Geisler, P. Kratzer, and V. Popescu, *Phys. Rev. B* **89**, 184422 (2014).
- [29] B. Geisler and P. Kratzer, *Phys. Rev. B* **92**, 144418 (2015).
- [30] B. Geisler and P. Kratzer, *Phys. Rev. B* **99**, 155433 (2019).
- [31] P. E. Blöchl, *Phys. Rev. B* **50**, 17953 (1994).
- [32] H. J. Monkhorst and J. D. Pack, *Phys. Rev. B* **13**, 5188 (1976).
- [33] M. Methfessel and A. T. Paxton, *Phys. Rev. B* **40**, 3616 (1989).
- [34] M. Hayward and M. Rosseinsky, *Solid State Sci.* **5**, 839 (2003).
- [35] K.-W. Lee and W. E. Pickett, *Phys. Rev. B* **70**, 165109 (2004).
- [36] R. Pentcheva and W. E. Pickett, *Phys. Rev. B* **78**, 205106 (2008).
- [37] R. Pentcheva, M. Huijben, K. Otte, W. E. Pickett, J. E. Kleibecker, J. Huijben, H. Boschker, D. Kockmann, W. Siemons, G. Koster, H. J. W. Zandvliet, G. Rijnders, D. H. A. Blank, H. Hilgenkamp, and A. Brinkman, *Phys. Rev. Lett.* **104**, 166804 (2010).
- [38] A. Blanca-Romero and R. Pentcheva, *Phys. Rev. B* **84**, 195450 (2011).
- [39] M. Wu, E. Benckiser, M. W. Haverkort, A. Frano, Y. Lu, U. Nwankwo, S. Brück, P. Audehm, E. Goering, S. Macke, V. Hinkov, P. Wochner, G. Christiani, S. Heinze, G. Logvenov, H.-U. Habermeier, and B. Keimer, *Phys. Rev. B* **88**, 125124 (2013).
- [40] F. Belviso, V. E. P. Claerbout, A. Comas-Vives, N. S. Dalal, F.-R. Fan, A. Filippetti, V. Fiorentini, L. Foppa, C. Franchini, B. Geisler, L. M. Ghiringhelli, A. Groß, S. Hu, J. Íñiguez, S. K. Kauwe, J. L. Musfeldt, P. Nicolini, R. Pentcheva, T. Polcar, W. Ren, F. Ricci, F. Ricci, H. S. Sen, J. M. Skelton, T. D. Sparks, A. Stroppa, A. Urru, M. Vandichel, P. Vavassori, H. Wu, K. Yang, H. J. Zhao, D. Puggioni, R. Cortese, and A. Cammarata, *Inorg. Chem.* **58**, 14939 (2019).
- [41] M. T. Curnan and J. R. Kitchin, *J. Phys. Chem. C* **118**, 28776 (2014).
- [42] L. Yu and A. Zunger, *Nat. Commun.* **5**, 5118 (2014).
- [43] A. Malashevich and S. Ismail-Beigi, *Phys. Rev. B* **92**, 144102 (2015).
- [44] J.-F. Ge, Z.-L. Liu, C. Liu, C.-L. Gao, D. Qian, Q.-K. Xue, Y. Liu, and J.-F. Jia, *Nat. Mater.* **14**, 285 (2015).